inter.noise
HAMBURG 2016

Study on Acoustic, Vibration and Flow Induced Noise Characteristics of T-shaped rectangular cross-sectional pipe

Masaaki Mori[1]; Takayuki Masumoto[1]; Kunihiko Ishihara[2]

[1] Cybernet Systems CO., LTD, Japan

[2] Tokushima Bunri University, Japan

ABSTRACT

An aerodynamic sound generated by flow inside a pipe is one of the noise problems. Aerodynamic sound sources are generated by the flow inside the pipe. However, in addition to the aerodynamic sound sources, a characteristic of the generated sound is sometimes affected by acoustic and vibration characteristics of the pipe. In this paper, we have performed the experiments and simulations to clarify acoustic, vibration and aerodynamic sound characteristics of a T-shaped rectangular cross-sectional pipe. Thicknesses of the pipe are 5mm and 2mm. The experiments and simulations were performed under several inflow velocity conditions. The results show that the characteristic of the generated aerodynamic sound in the pipe is strongly affected by both acoustic and vibration characteristics of the pipe, especially in the case that the thickness is 2mm. Frequency characteristics of the generated sound sources depend on the inflow velocity conditions. However, those of the generated sound do not depend on the inflow velocity conditions, but on the acoustic and vibration frequency characteristics of the pipe.

Keywords: Flow-induced noise, BEM, Acoustic Characteristics, Structure-Acoustic Coupling I-INCE Classification of Subjects Number(s): 21.6

1. INTRODUCTION

An aerodynamic sound generated by a flow inside a pipe or a duct is one of the noise problems in the equipment such as air conditioner. An air conditioner consists of a duct, fan and openings. There are three types of flow-induced sound sources in the air conditioner. One is the sound sources generated by the fan, so-called fan noise. The second is the sound sources generated by the flow around bending or expanding parts of the duct. The third is the sound sources generated by the flow near openings. However, it is still incompletely understood that which type of the sound sources is dominant. In order to reduce the noise, it is necessary to know the dominant sound sources.

Studies on the aerodynamic sound generated inside the duct have been done experimentally. Watanabe et al. investigated the acoustic power level generated by the air flow in duct systems (1). Itamoto and Shiokawa studied flow noise and sound characteristics of glass fiver ducts (2, 3). Their research results are also used as data collection. Ishihara investigated acoustic and flow noise characteristics of straight and bending duct with some openings (4, 5, 6). It is clarified that the noise reduction effect of the absorbing treatment could be neglected when noise sources were generated only by the flow. The noise reduction effects due to bending and use of inner guides or airfoils were clarified. In the case of pipe noise, Hambric et al. studied the flow-induced vibration and acoustic power spectra of a 90^o piping elbow and proposed a procedure of the coupling of CFD and structural-acoustic models (7). Zhang et al. studied the flow-induced vibration and noise of a 90^o piping elbow and the effect of guide vanes (8). They computed the hydrodynamic noise based on a hybrid LES/Lighthill's acoustic analogy (9) and clarified the effective position of guide vanes in reducing vibration and flow-induced noise in the 90^o piping elbow with water. However, to the author's knowledge, there have not been many studies focused on effects of both acoustic

[1] m-mori@cybernet.co.jp [3] k-ishihara@fe.bunri-u.ac.jp

[2] masumoto@cybernet.co.jp

and vibration characteristics of pipes on aerodynamic sounds.

The purpose in this paper is to clarify the effect of the acoustic and vibration characteristics of the pipe on the aerodynamic sound. We have performed both experiments and simulations of aerodynamic sounds generated by the flow in the T-shaped pipe with the square cross-section in cases of 5mm and 2mm pipe thickness. To predict aerodynamic sounds computationally, the hybrid CFD/BEM method (10, 11) is applied. The mode shapes are calculated by means of FEM, and the acoustic characteristics are calculated by means of BEM including the structure-acoustic coupling effect. In our previous work (12), the effect of the structure vibration on the far-field sound pressure is relatively small in the case of 5mm pipe thickness. The frequency characteristics of the aerodynamic sound in the pipe are affected mainly by the acoustic frequency charecteristic of the pipe interior sound field. In this paper, the effect of the pipe thickness on the acoustic and vibration characteristics of the pipe and the results of the structure–acoustic coupling simulation using the acoustic sources extracted from CFD results for the case of 2mm pipe thickness will be discussed.

2. EXPERIMENT

2.1 Experimental Setup

Experimental setup is shown in Fig. 5. With a microphone that is placed at 100mm from the centre of the outflow boundary, sound pressure signals are measured and converted to frequency domain with FFT Analyzer. The frequency range is from 20Hz to 1000Hz, the sampling frequency is 10000Hz, the number of averages is 1000, and the frequency resolution is 10Hz. Inflow velocities are about 6, 8, 12m/s. Background sound pressure level is below 30dB.

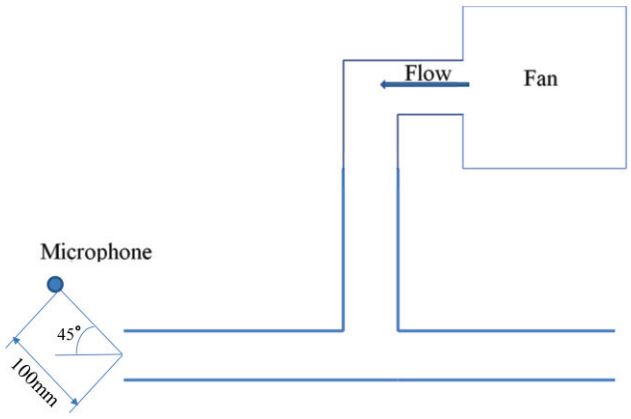

Figure 1 – Experimental setup

2.2 Experimental Results

Figure 2 shows the frequency spectra of SPL at the monitor point. Those for 5mm and 2mm pipe thickness cases are shown in Fig. 2(a) and (b), respectively. As shown in Fig.2, depending on the inflow velocity, magnitudes of the sound pressure are different for all inflow velocities. However, the frequency characteristics of SPL do not depend on the inflow velocity, and peak frequencies of SPL are almost the same for all inflow velocities (12).

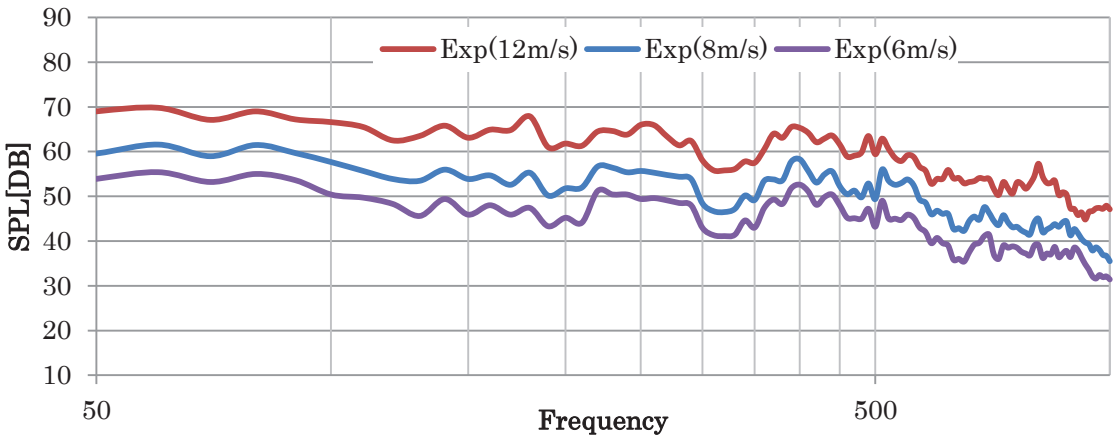

(a) Spectrum of sound pressure levels for 5mm thickness case

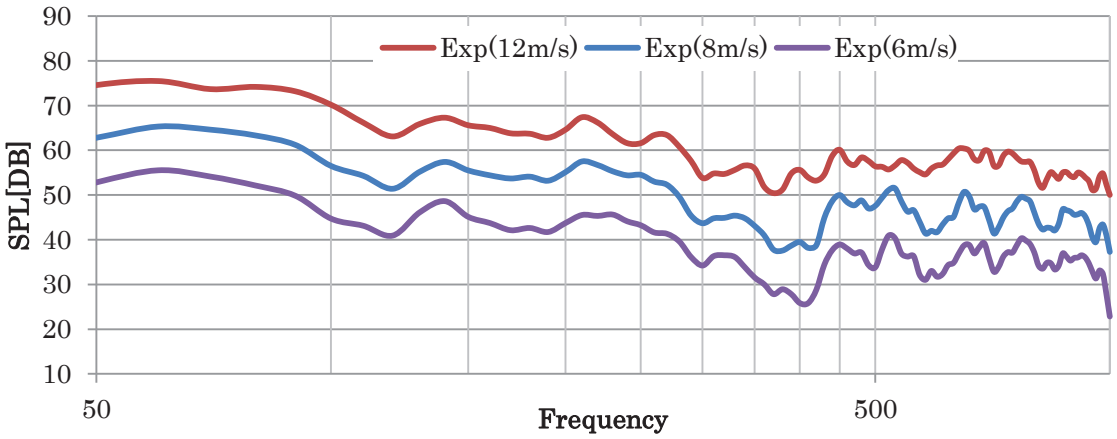

(b) Spectrum of sound pressure levels for 2mm thickness case

Figure 2 – Spectrum of sound pressure levels

Figure 3 shows the comparison of the sound pressure level between 5 mm and 2 mm pipe thickness cases. The frequency characteristics of SPL strongly depend on the thickness of the pipe, and those are different at the frequency ranges from 150 Hz to 1000Hz between 5 mm and 2 mm pipe thickness cases. It can be presumed that the vibration characteristic of the pipe affect the aerodynamic sound in the case of 2mm pipe thickness.

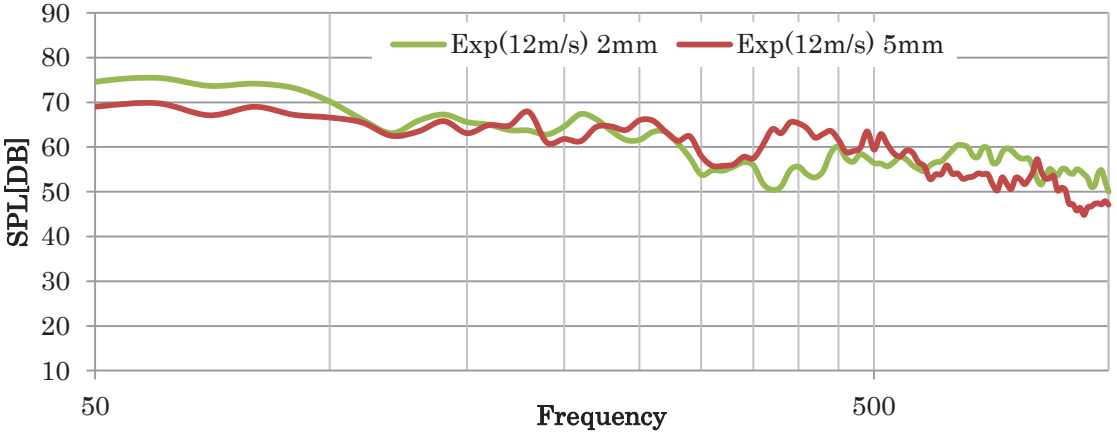

Figure 3 – Comparison of SPL between 5 mm and 2 mm thickness cases at 12 m/s

3. NUMRICAL PROCUDURE

3.1 Transient CFD simulation

The transient flow fields in the T-shaped rectangular cross-sectional pipe of diameter D = 100 mm are simulated at Reynolds numbers, Re = 41075 and 78728. Inflow velocities are U = 6 and 12 m/s. The model used for the CFD simulation is shown in Fig. 4. For this simulation, a three-dimensional computational domain in the T-shaped rectangular cross-sectional pipe has been applied. Unsteady flow fields are calculated using the CFD code ANSYS Fluent version 15.0 and its incompressible LES (Dynamic Smagorinsky model) calculation features. The origin of the Cartesian coordinate is placed at the midpoint of the pipe. The domain contains 544,000 hex cells and 573,221 nodes. Steady velocities are imposed on the inflow boundary. Zero pressure outflow conditions are applied on the outflow boundaries. No-slip conditions are applied on the other walls. Steady state simulations were performed and used as initial conditions of transient simulations. The transient simulations were performed for 7,800 time steps with a time step size Δt = 1e-4 s.

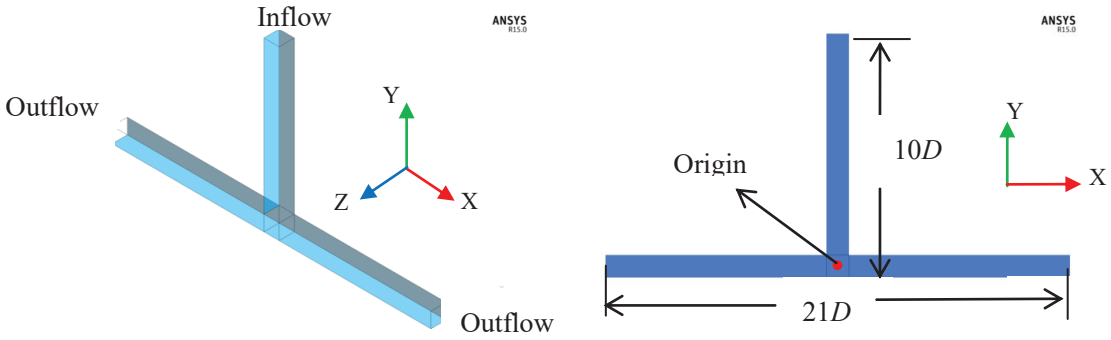

Figure 4 – Domain shape and schematic diagram

3.2 Lighthill Equations

Lighthill equation (13, 14) in the frequency domain is derived from the equation of continuity and compressible Navier-Stokes equation and as follows:

$$(\nabla^2 + k^2)p = -\frac{\partial^2 T_{lm}}{\partial x_l \partial x_m}\ , \tag{1}$$

where p is the acoustic pressure, k is the wave number, c is the speed of sound, l and m indicate each direction in the Cartesian coordinates, v is the flow velocity. T_{lm} is the Lighthill stress tensor and as follows:

$$T_{lm} = \rho v_l v_m + (p - c^2\rho)\delta_{lm} - \tau_{lm}, \tag{2}$$

where ρ is the density and 1.225kg/m^3, δ_{ij} is the Kronecker delta and τ_{lm} is the viscous stress tensor. For a low Mach number and high Reynolds number flow regime, the second and third terms of equation (2) are negligible (8, 10, 15). Therefore, the first term is used for the present work.

3.3 Extraction of Acoustic Source Data

To convert the acoustic source time histories into the frequency spectra, the discrete Fourier transform (DFT) has been applied. The acoustics sources are extracted from 512 steps (from t = 0.52s to 0.6222s) flow field data, the sampling period is 2e-4s.

3.4 Acoustic Simulation

The acoustic characteristics are solved using the commercial BEM code WAON. In this solver, the following simultaneous linear equation is solved:

$$(\boldsymbol{E} + \boldsymbol{B} + \boldsymbol{C})\boldsymbol{p} = j\omega\rho\boldsymbol{A}\boldsymbol{v} + \boldsymbol{p}_{\mathrm{d}}, \tag{3}$$

Here, $\boldsymbol{p}$ is the acoustic pressure vector, $\boldsymbol{v}$ is the particle velocity vector and the entries of the influence coefficient matrices are represented as follows:

$$E_{ij} = \frac{1}{2}\delta_{ij}, \tag{4}$$

$$A_{ij} = \int_{\Gamma_V} N_j(\boldsymbol{r}_q) G(\boldsymbol{r}_i, \boldsymbol{r}_q) dS_q, \tag{5}$$

$$B_{ij} = \int_{\Gamma} N_j(\boldsymbol{r}_q) \frac{\partial G(\boldsymbol{r}_i, \boldsymbol{r}_q)}{\partial n_q} dS_q, \tag{6}$$

$$C_{ij} = \frac{jk}{Z_j} \int_{\Gamma_A} N_j(\boldsymbol{r}_q) G(\boldsymbol{r}_i, \boldsymbol{r}_q) dS_q, \tag{7}$$

where δ_{ij} is Kronecker delta, and Γ is the total boundary. Γ_V is a part of Γ where the surface is assumed to be vibrating. Γ_A is also a part of Γ where the surface absorbs acoustic wave. $\boldsymbol{r}_i$ is a position vector of the i-th node, $\boldsymbol{r}_q$ is a position vector of the source point q, and N_j is the interpolation function of the j-th node. With the number of nodes N, the component p of the vector $\boldsymbol{p}$ is as follows:

$$p(\boldsymbol{r}_q) = \sum_{j=1}^{N} N_j(\boldsymbol{r}_q) p_j. \tag{8}$$

The component p_d of the vector $\boldsymbol{p}_d$ is the direct pressure contribution from the acoustic source, which is evaluated by the following equation:

$$p_d(\boldsymbol{r}_p) = \frac{1}{4\pi} \frac{\partial^2}{\partial x_l \partial x_m} \int_{-\infty}^{\infty} \frac{T_{lm}(\boldsymbol{r}_s, \omega) e^{jk|r_p - r_s|}}{|\boldsymbol{r}_p - \boldsymbol{r}_s|} dV \tag{9}$$

where $\partial^2/\partial x_l \partial x_m$ is the directional derivative and V is the volume of the flow field (in this case, the region filled by CFD cell). $\boldsymbol{r}_p$ is a position vector of the monitor point p, and $\boldsymbol{r}_s$ is a position vector of the source points.

There are 2,780 boundary elements. The acoustic sources are extracted from CFD results, whose numbers are equivalent to the number of grids of the CFD model. Figure 5 shows the boundary elements. To concern acoustic waves moving from the inflow boundary to the outside, an impedance boundary condition is imposed at the inflow boundary. The value of the impedance is ρc. In the structure-acoustic coupled model, all surfaces other than inflow boundary are boundaries where the structure-acoustic coupling effect is considered. In the uncoupled model, they are assumed to be rigid.

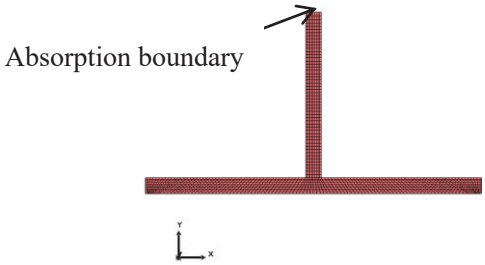

Figure 5 – Boundary element mesh

3.5 Structural-Acoustic Coupling

In this paper, the structural-acoustic coupled model is solved. In order to solve structural-acoustic coupled model, equations corresponding to the acoustic field and structure must be solved simultaneously.

Displacement of the structure is described using equation of motion as follows:

$$(-\omega^2 \boldsymbol{M} + j\omega \boldsymbol{C} + \boldsymbol{K})\boldsymbol{u} = \boldsymbol{f}_s, \tag{10}$$

where $\boldsymbol{M}$ is the Mass matrix, $\boldsymbol{C}$ is the Damping matrix, $\boldsymbol{K}$ is the Stiffness matrix and $\boldsymbol{f}_s$ is the excitation force vector. With modal coordinates, Equation (10) is expressed as follows:

$$(-\omega^2 + 2jh\omega\boldsymbol{\omega}_0 + \boldsymbol{\omega}_0^2)\boldsymbol{q} = \boldsymbol{\varphi}^T \boldsymbol{f}_s, \tag{11}$$

where h is the modal damping ratio, $\boldsymbol{\omega}_0$ is the matrix in which eigenvalues are arranged diagonally, $\boldsymbol{\varphi}^T$ the eigenvector transposition, and $\boldsymbol{q}$ the modal participation factor.

In order to consider the acoustic contribution to the structural model, an additional force term from the

acoustic field is introduced as follows:

$$(-\omega^2 + 2jh\omega\boldsymbol{\omega}_0 + \boldsymbol{\omega}_0^2)\boldsymbol{q} = \boldsymbol{\varphi}^{\mathrm{T}}(\boldsymbol{f}_{\mathrm{s}} - \boldsymbol{p}s), \tag{12}$$

where s is the area affected by the acoustic pressure.

On the other hand, to consider the structural contribution to the acoustic model, an additional velocity term from the structure is introduced to Equation (3):

$$(\boldsymbol{E} + \boldsymbol{B} + \boldsymbol{C})\boldsymbol{p} = j\omega\rho\boldsymbol{A}\boldsymbol{v} + j\omega\rho\boldsymbol{A}'\boldsymbol{v}_{\mathrm{s}} + \boldsymbol{p}_{\mathrm{d}}, \tag{13}$$

here $\boldsymbol{v}_{\mathrm{s}}$ the vibration velocity vector of the structural model and,

$$A'_{ij} = \int_{\Gamma_3} N_j(\boldsymbol{r}_q)G(\boldsymbol{r}_i, \boldsymbol{r}_q)dS_q, \tag{14}$$

where Γ_3 is the boundary on which structural-acoustic coupling effect is considered. Γ_3 corresponds to all of the surfaces other than the inflow boundary in Fig.5.

The term $\boldsymbol{v}_{\mathrm{s}}$ in Equation (13) is modified into an expression in which modal coordinates are used. Combining Equation (12) and (13), we obtain the following coupled equation of acoustic and structural models:

$$\begin{bmatrix} \boldsymbol{E} + \boldsymbol{B} + \boldsymbol{C} & \omega^2\rho\boldsymbol{A}'\boldsymbol{\varphi} \\ -\boldsymbol{\varphi}^{\mathrm{T}}s & -\omega^2 + 2jh\omega\boldsymbol{\omega}_0 + \boldsymbol{\omega}_0^2 \end{bmatrix} \begin{Bmatrix} \boldsymbol{p} \\ \boldsymbol{q} \end{Bmatrix} = \begin{Bmatrix} j\omega\rho\boldsymbol{A}\boldsymbol{v} + \boldsymbol{p}_{\mathrm{d}} \\ \boldsymbol{\varphi}^{\mathrm{T}}\boldsymbol{f}_{\mathrm{s}} \end{Bmatrix}. \tag{15}$$

The modal information of the pipe has been extracted using ANSYS Mechanical version 15.0. Figure 6 shows boundary conditions in the modal analysis.

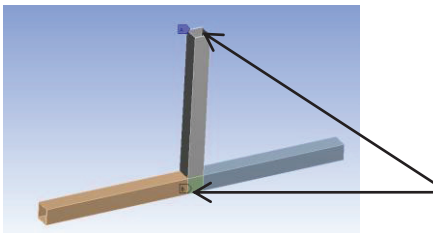

Figure 6 – Boundary conditions in the modal analysis

Young's Modulus, Poisson's ratio and density of the T-rectangular pipe are respectively, 3.14GPa, 0.35 and 1190kg/m^3. The damping ratio is 0.05 (5%). Thicknesses of the pipe are 5mm and 2mm. As the results of the modal analysis, typical mode shapes are obtained, as shown in Figs.7 and 8.

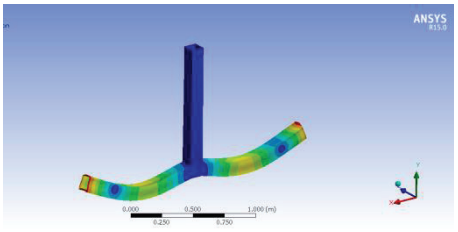

10th mode at f = 190.31 Hz

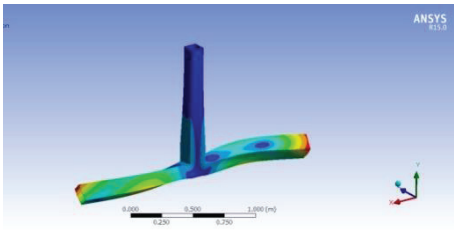

11th mode at f = 190.35 Hz

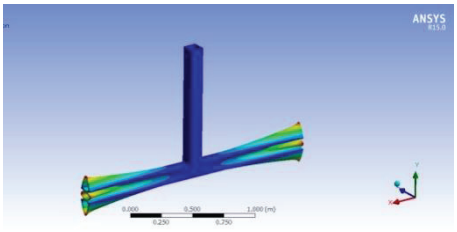

21st mode at f = 353.76 Hz

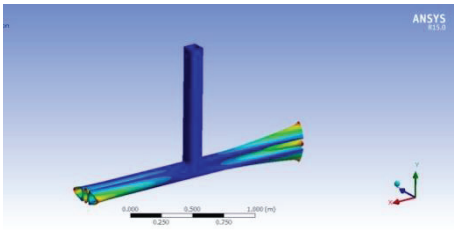

22nd mode at f = 353.76 Hz

Figure. 7 –Mode shapes for 5mm pipe thickness

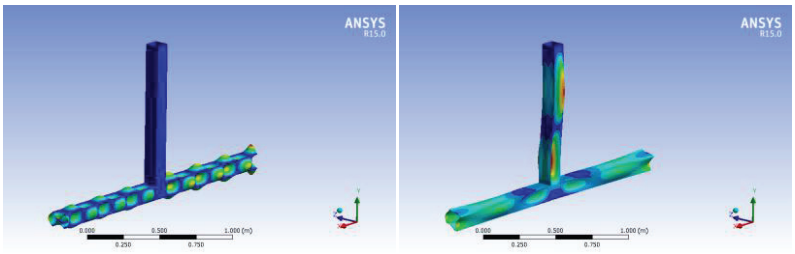

37th mode at f = 255.49 Hz 38th mode at f = 260.76 Hz

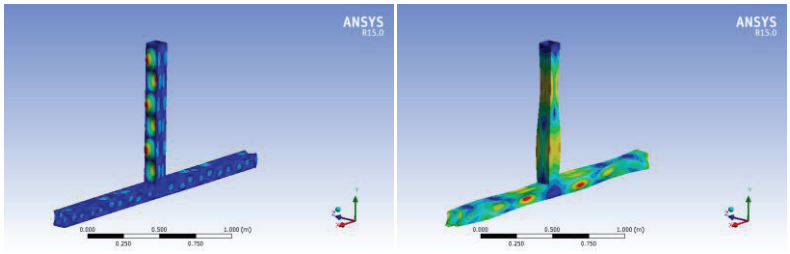

73th mode at f = 348.79 Hz 100th mode at f = 351.48 Hz

Figure. 8 –Mode shapes for 2mm pipe thickness

4. STRUCTURE – ACOUSTIC COUPLING SIMULATION WITHOUT CFD RESULTS

4.1 Acoustic Sources

As shown in Fig. 2, peak frequencies of SPL do not depend on the inflow velocity. Therefore, it can be presumed that acoustic modes of the pipe interior sound field or vibration modes of the pipe strongly affect the frequency characteristics of the flow-induced sound in the pipe. To clarify acoustic and vibration characteristics of the pipe, the acoustic frequency responses have been calculated using the monopole point sources (without the flow) shown in Fig. 9 with/without the structure-acoustic coupling. To examine the position dependence of the sound source, two types of analysis models are used, as shown in Fig. 9. In the case of Type 1, the point source is located at the origin ("Symmetric source" position case). In the case of Type 2, the point source is located at (4D, 0, 0) ("Asymmetric source" position case). The magnitude of the point sources is 1Pa in all frequencies.

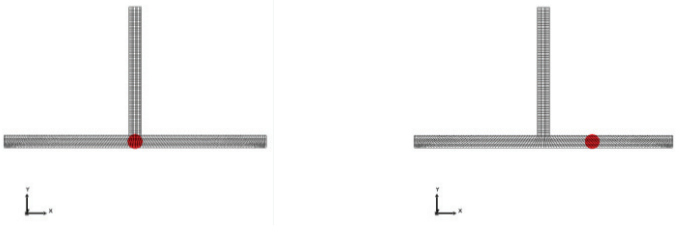

(a) Type1 ("Symmetric source" case) (b) Type2 ("Asymmetric source" case)

Figure. 9 – Acoustic sources for the frequency response analysis

4.2 Acoustic and Vibration Characteristics of Pipe

Figure 10 shows acoustic frequency charecteritics of the pipe (without the flow). Figure 10 shows the comparison of sound pressure levels in the cases of the coupled and uncoupled model. The measured data (with the flow) is also plotted in Fig. 10. The results for the cases of 5mm and 2mm pipe thickness are shown Fig. 10(a) and (b), and Fig. 10(c) and (d), respectively. In the case of 5mm pipe thickness, there is no significant difference between the coupled and uncoupled models in terms of the frequency characteristics of the far-field sound pressure, as shown in Figs. 10 (a) and (b). It

indicated that the effect of the structure vibration on the far-field sound pressure is relatively small in the case of 5mm pipe thickness (12). In the case of 2mm pipe thickness, Fig. 10 (c) and (d) show that there are significant differences between the coupled and uncoupled models. Some peak frequencies of the coupled model are different from those of the uncoupled model, and the frequency characteristics of the coupled model are similar to the measured data (with the flow), as shown in Fig. 10 (c) and (d). It indicated that the effect of the structure vibration on the far-field sound pressure is large in the case of 2mm pipe thickness.

Some outstanding peaks are surrounded by red and blue circles in Fig. 10(a), (b), (c) and (d). Figure 10 show that in the case of Type 2, more acoustic modes are excited than in the case of Type 1. Comparing the cases of Type 1 and Type 2, in the case of Type 1, the simulated data is smooth and similar to the measured data (with the flow). However, in the case of Type 2, some acoustic modes (peaks surrounded by the red circle) appear and their modes also appear in the measured data. The results show that the acoustic frequency characteristics of the pipe depend on the position of the acoustic source, and are similar to the frequency characteristics of the flow-induced sound in the pipe in terms of the peak frequency for both cases of 5mm and 2mm thickness. Figure 10(c) and (d) suggest that the frequency characteristic of the far-field sound pressure is strongly affected by the structure vibration of the pipe in addition to the acoustic frequency characteristic of the pipe interior sound field in the case of 2 mm thickness.

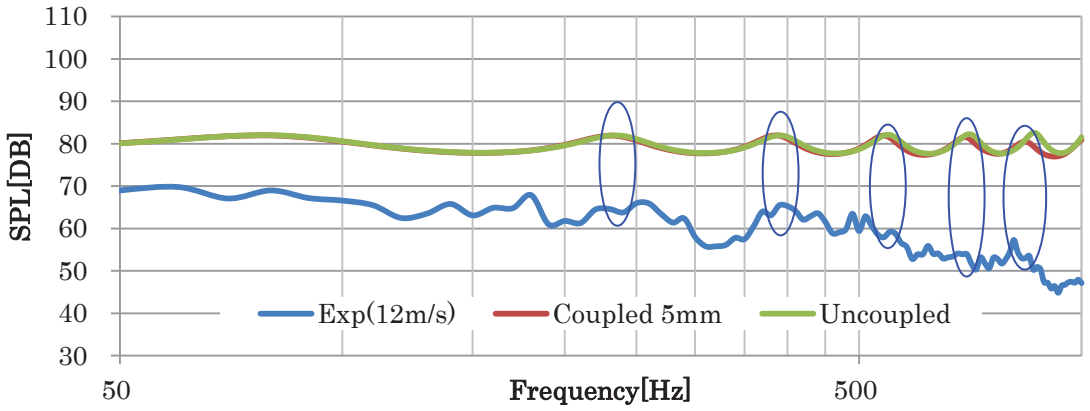

(a) Type 1 (“Symmetric source” case) for 5mm pipe thickness

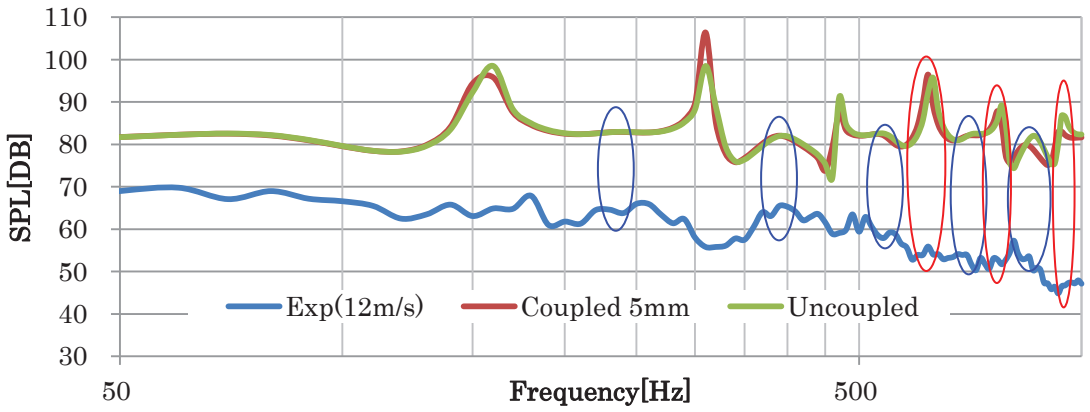

(b) Type 2 (“Asymmetric source” case) for 5mm pipe thickness

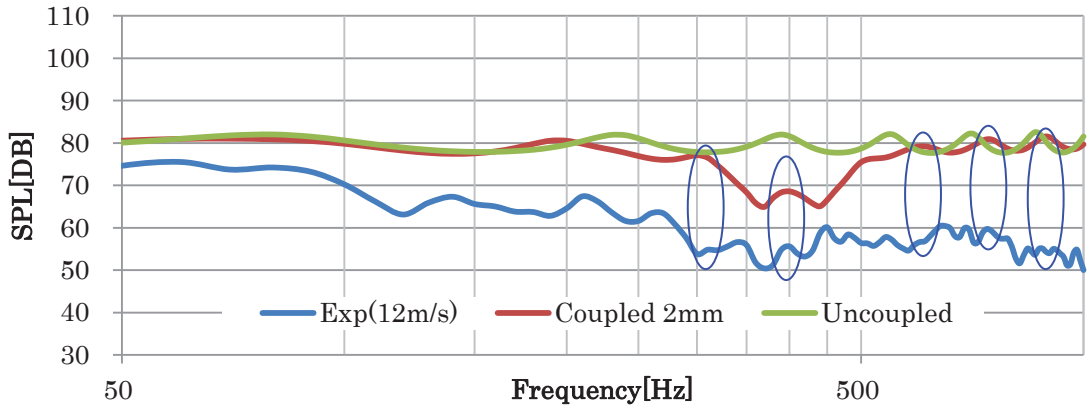

(c) Type 1 ("Symmetric source" case) for 2mm pipe thickness

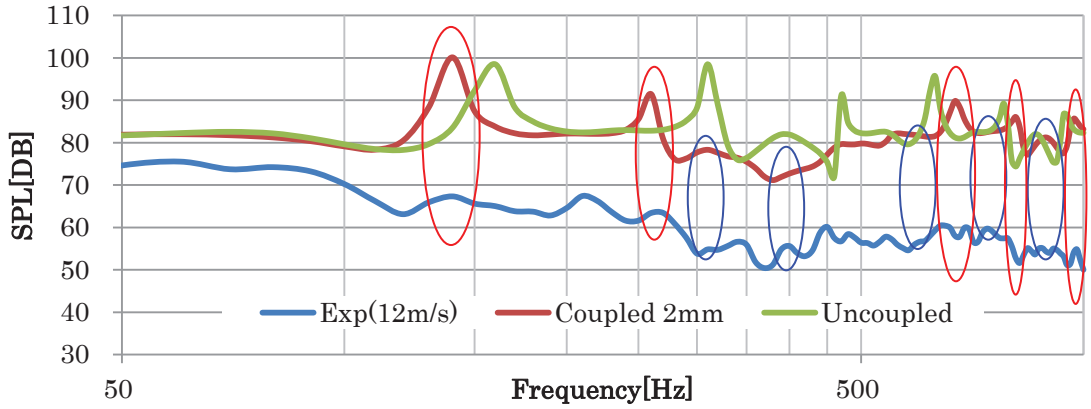

(d) Type 2 ("Asymmetric source" case) for 2mm pipe thickness

Figure 10 – Acoustic frequency characteristics of the pipe (without the flow)

5. STRUCTURE – ACOUSTIC COUPLING SIMULATION WITH CFD RESULTS

5.1 Transient CFD Results

Figure 11 shows the magnitude of the volumetric acoustic sources (Lighthill stress tensor) extracted from the CFD results at 310 Hz. Significant acoustic sources exist near corners and the wall of the pipe in Fig. 11. As shown in Fig. 11, magnitudes of the acoustic sources are relatively symmetry with respect to the YZ plane. The frequency spectra of the volumetric Lighthill stress tensor $\rho v_1 v_1$ at $(1D, 0, 0)$ are shown in Fig. 12. Figure 12 show that the peak frequencies of the acoustic sources depend on the inflow velocity.

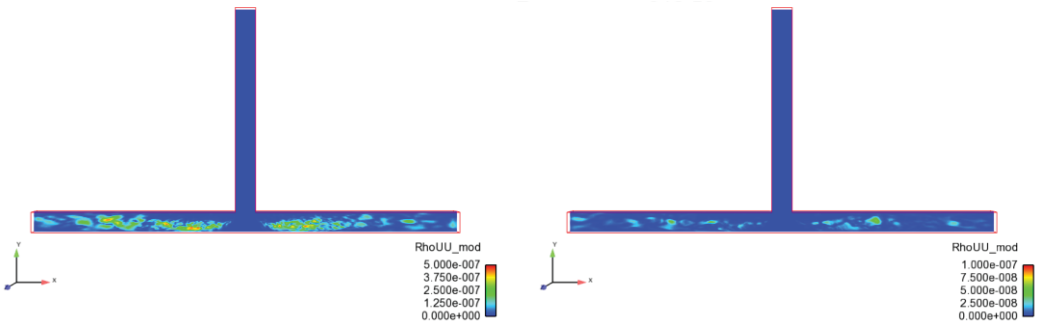

Figure 11 – Magnitude of volumetric acoustic sources $\rho v_l v_m$ at z=0 plane (left: 12 m/s, right: 6 m/s)

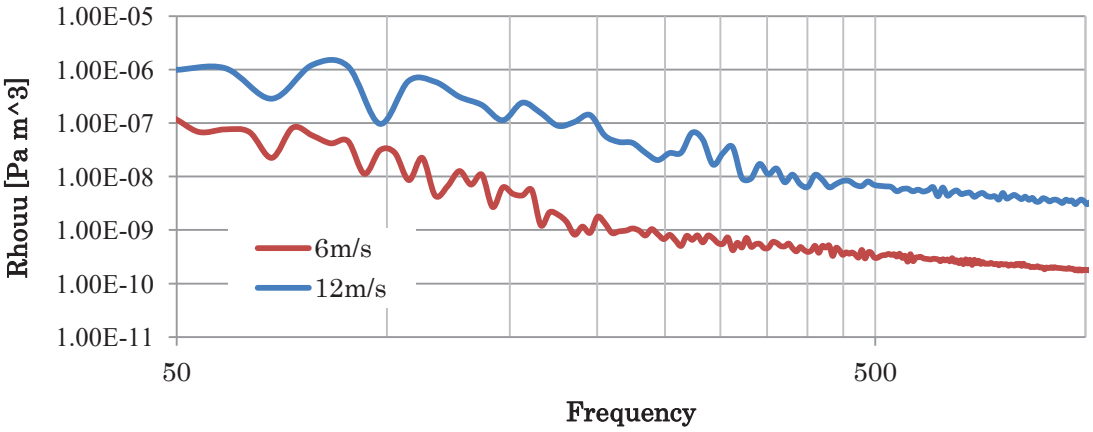

Figure 12 – Spectrum of volumetric Lighthill stress tensor ρuu

5.2 Far-Field Acoustics

To investigate the effect of the structural-acoustic coupling on the far-field sound pressure, we have calculated flow-induced sound pressure fields in both cases of the coupled and uncoupled model using the acoustic sources extracted from the CFD results for the case of 2mm pipe thickness. Figure 13 shows the comparison of sound pressure levels in the cases of the coupled and uncoupled model for the case of 2mm pipe thickness. The position of the monitor point is shown in Fig. 1. Clearly, there are significant differences between the coupled and uncoupled models in terms of the frequency characteristics of the far-field sound pressure, as in Fig. 10. Comparing the coupled model with the uncoupled model, the frequency characteristics of the coupled model are similar to the measured data (with the flow), as shown in Fig. 13. Figure 14 shows contours of the sound pressure field in both cases of the coupled and uncoupled model. Also, the directivity of the sound pressure in the case of the coupled model is different from that in the case of the uncoupled model. It indicated that the directivity of the sound pressure is strongly affected by the structural vibration in the case of coupled model.

Figure 15 shows the frequency spectra of SPL at the position for the case of 2mm pipe thickness. Both the simulated and measured data are shown in Fig. 15. As shown in Fig.12, the frequency characteristics of the acoustic sources depend on the inflow velocity. However, both the measured and simulated frequency characteristics of SPL do not depend on the inflow velocity, and peak frequencies of SPL are almost the same between 12 m/s and 6 m/s cases, as shown in Figs. 2 and 15. This is due to the fact that the frequency characteristics of the flow-induced sound in the pipe is affected by the acoustic and vibration frequency charecteristics of the pipe, as shown in Fig. 10. Figure 16 shows contours of the sound pressure field for the case of 2mm pipe thickness at U=12 m/s and 6 m/s. This figure shows that magnitudes of the sound pressure are different between U=12 m/s and 6 m/s cases depending on the inflow velocity. This figure also shows that directivities of the far-field sound pressure are affected by the structural vibration in the two cases.

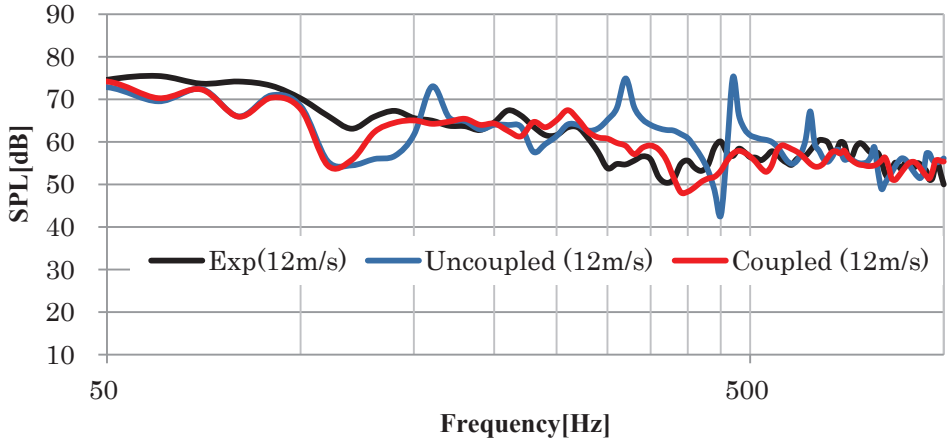

Figure 13 – Comparison of SPLs in the cases of the coupled and uncoupled models at U = 12m/s

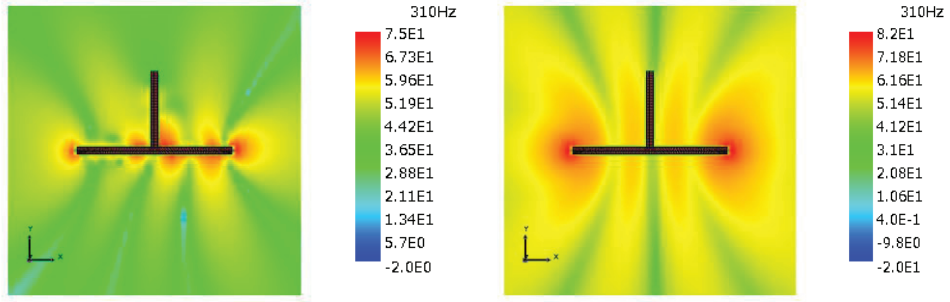

Figure 14 – Sound pressure field at z=0 plane at U=12 m/s (Left: Coupled model, Right: Uncoupled model)

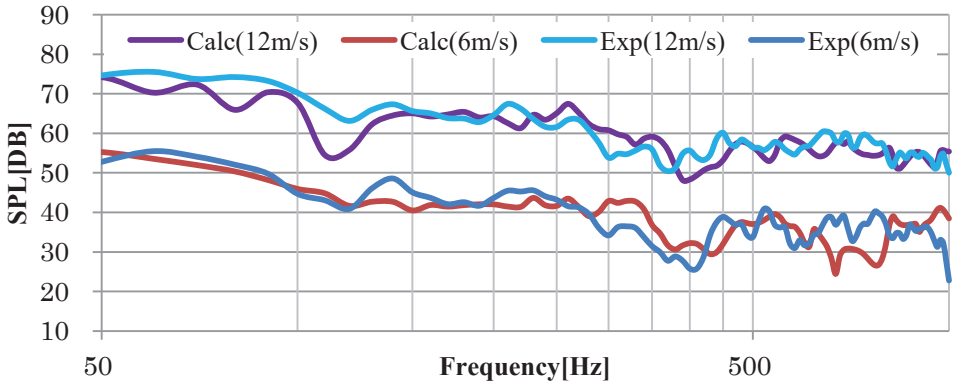

Figure 15 – Spectrum of SPL near the outflow boundary

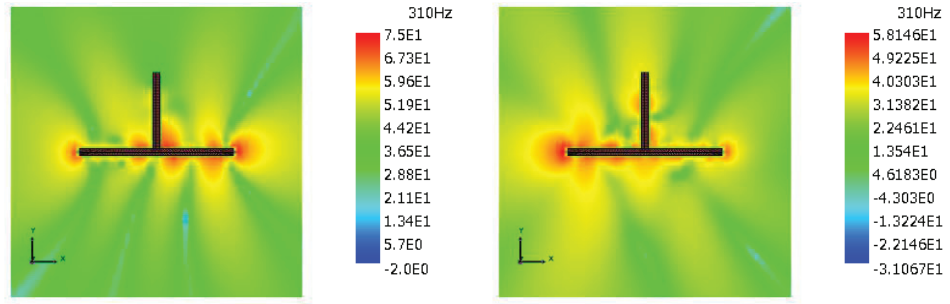

Figure 16 – Sound pressure field at z=0 plane (Left: U = 12m/s, Right: U=6m/s)

6. CONCLUSIONS

In this paper, we have performed the experiments and simulations on the acoustic, vibration and aerodynamic sound characteristics of the T-shaped rectangular cross-sectional pipe in cases of 5mm and 2mm pipe thickness. We have analysed the effect of the pipe thickness on the acoustic and vibration characteristics of the pipe. The following concluding remarks are obtained in this paper.

1. The acoustic frequency responses of the pipe interior sound field were calculated using two types of the monopole point sources (without the flow) with/without the structural-acoustic coupling. In terms of the frequency characteristics of the sound pressure, the structural – acoustic coupling effect on the far-field sound pressure is relatively small for the case of 5mm pipe thickness. However, it is large for the case of 2mm pipe thickness.

2. The acoustic frequency characteristics of the pipe depend on the position of the acoustic source. They are similar to the frequency characteristics of the flow-induced sound in the pipe in terms of the peak frequency. The results explain that the frequency characteristics of the flow-induced sound in the pipe are affected mainly by the acoustic frequency characteristic of the pipe for the case of 5mm thickness,

and they are affected by both acoustic and vibration characteristics of the pipe for the case of 2mm thickness.

3. Flow-induced sound pressure fields were calculated using the acoustic sources extracted from the CFD results with/without the structural-acoustic coupling effect for the case of 2mm pipe thickness. The results explain that frequency characteristics and directivities of the flow-induced sound in the pipe are strongly affected by the structural vibration in addition to the acoustic frequency characteristic of the pipe interior sound field.

REFERENCES

1. Watanabe K et al. A Study on Noise Generated by the Air Flow in Duct System. Journal of the Society of Heating, Air-Conditioning and Sanitary Engineers of Japan. 1963;37(5): 22-33.
2. Shiokawa, H, Itamoto, M. On Sound Characteristics of Straight Glass Fiber Ducts. Journal of Architecture, Planning and Environmental Engineering, Architectural Institute of Japan. 1993;435: 9-15.
3. Itamoto M, Shiokawa H. On Generated Noise by Air Flow at Straight Glass Fiber Ducts. Journal of Architecture, Planning and Environmental Engineering, Architectural Institute of Japan. 1991;428: 21-27.
4. Ishihara K. Study on Acoustics Characteristics of Straight Duct with Some Holes. Transactions of the Japan Society of Mechanical Engineers. 2008;74:332-338.
5. Ishihara K. Flow Noise Characteristics Generated from Straight Duct with Some Holes. Transactions of the Japan Society of Mechanical Engineers. 2009;74:2521-2528.
6. Ishihara K. Study on Acoustics and Flow Noise Characteristics of Bending Duct. Transactions of the Japan Society of Mechanical Engineers. 2011;77:1282-1291.
7. Hambric S. A., Boger D. A., Fahnline J. B. Campbell R. L. Structure- and fluid-borne acoustic power sources induced by turbulent flow in 90° piping elbows. Journal of Fluids and Structures. 2010;26:121-147.
8. Zhang T., Zhang Y., Ouyang H. Structural vibration and fluid-borne noise induced by turbulent flow through a 90 piping elbow with/without a guide vane. International Journal of Pressure Vessels and Piping. 2015:66-77.
9. Zhang Y., Zhang T., Ouyang H., Li, T. Y. Flow-induced noise analysis for 3D trash rack based on LES/Lighthill hybrid method. Applied Acoustics. 2014;77:141-152.
10. Croaker P, Kessissoglou N, Marburg S. A CFD-BEM coupling technique for low Mach number flow induced noise. Proceedings of Acoustics 2013; Victor Harbor, Australia 2013.
11. Mori M, Masumoto T, Ishihara, K, Oshima T, Yasuda Y, Sakuma T. Study on modeling of flow induced noise using Lighthill's analogy and boundary element method. Proceedings of Internoise 2014; Melbourne, Australia 2014.
12. Mori M, Masumoto T, Ishihara, K. Study on Acoustic and Flow Induced Noise Characteristics of T-Shaped Pipe with Square Cross-Section. Advances in Applied Acoustics (AIAAS) 2016;5:10-17
13. Lighthill, Michael James. On sound generated aerodynamically, I. General theory. Proceedings of the Royal Society of London Series A. 1952;211:564-587.
14. Lighthill, Michael James. On sound generated aerodynamically, II. Turbulence as source of sound. Proceedings of the Royal Society of London Series A. 1954;222:1-32.
15. Howe, Michael, S. Theory of Vortex Sound: Cambridge University Press; 2003.